INL/JOU-24-82208-Revision-0

Sensitivity study of hydrogen Soret transport in yttrium Hydride-Based nuclear fuel

July 2025

Jordan Andrew Evans, Chase N Taylor, Adrian R Wagner, Ryan Terrence Sweet, Travis Louis Lange, Nicolas E Woolstenhulme

Changing the World's Energy Future

INL is a U.S. Department of Energy National Laboratory operated by Battelle Energy Alliance, LLC

INL/JOU-24-82208-Revision-0

Sensitivity study of hydrogen Soret transport in yttrium Hydride-Based nuclear fuel

Jordan Andrew Evans, Chase N Taylor, Adrian R Wagner, Ryan Terrence Sweet, Travis Louis Lange, Nicolas E Woolstenhulme

July 2025

Idaho National Laboratory
Idaho Falls, Idaho 83415

http://www.inl.gov

Prepared for the
U.S. Department of Energy
Under DOE Idaho Operations Office
Contract DE-AC07-05ID14517

INL/JOU-24-82208

Sensitivity Study of Hydrogen Soret Transport in Yttrium Hydride-Based Nuclear Fuel

Jordan A. Evans[1*], Chase N. Taylor[1], Adrian R. Wagner[1], Ryan T. Sweet[1], Travis L. Lange[1], Nicolas E. Woolstenhulme[1]

[1] Idaho National Laboratory, P.O. Box 1625, Idaho Falls, ID 83415-3840
[*] Corresponding Author, J.A. Evans, jordan.evans@inl.gov

ORCiDs
J. Evans: 0000000263239815
C. Taylor: 0000000230633752
A. Wagner: 0000000289614759
R. Sweet: 0000000279194623
T. Lange: 0000000284888849
N. Woolstenhulme: 0000000278813314

Sensitivity Study of Hydrogen Soret Transport in Yttrium Hydride-Based Nuclear Fuel

Abstract
Yttrium hydride is an excellent solid neutron moderator material for high temperature nuclear reactor applications due to its high hydrogen density and exceptional hydride stability at high temperatures. Despite these attractive characteristics, the details of how hydrogen behaves within yttrium hydride while temperature gradients exist are still not well understood. The evolution of the hydrogen composition profile resulting from a temperature gradient requires knowledge of hydrogen's heat of transport, a critical parameter that has not yet been measured for this material. In this work, we perform hydride redistribution, hydrogen dissociation, and hydrogen leakage calculations while varying the Soret heat of transport of hydrogen in yttrium hydride to elucidate the sensitivity of hydride stability under temperature gradients to this parameter. This study analyzes hydride stability of a hypothetical uranium-yttrium hydride nuclear fuel design during operation of a high temperature liquid metal-cooled nuclear reactor. Assuming U-YH_x could be fabricated in a physically stabilized manner, this fuel system can likely maintain hydride stability while operating at very high power densities and temperatures. We find that even though the hydrogen dissociation pressure in the gas gap does vary by several percent as the heat of transport temperature parameter is varied, the hydrogen content in the U-YH_x fuel meat is relatively insensitive to this parameter over the course of a high burnup fuel cycle; this is due to yttrium hydride's excellent hydrogen retention under the high temperature conditions considered here. This suggests that hydride stability analyses are insensitive to the value of the Soret heat of transport in U-YH_x under steady state liquid metal-cooled reactor conditions. However, the susceptibility to internal gas overpressurization-induced stress-rupture of the cladding during a high temperature transient is more sensitive to this parameter due to the non-linear dependence of hydrogen gas dissociation pressure vs. composition and temperature.

Key words: yttrium hydride, Soret effect, heat of transport, nuclear fuel

1. INTRODUCTION

Hydrogen is extremely effective at slowing down neutrons born from fission. Most nuclear reactors use water as primary coolant which also serves as an effective neutron moderator due to its abundance of hydrogen. New thermal neutron spectrum reactor concepts are under consideration which would benefit from smaller, more light-weight neutron moderation, such as microreactors and space reactors. In mobile reactor concepts, minimizing volume and mass of the system is a high priority in order to achieve the desired thermal neutron spectrum while remaining transportable, prohibiting the use of water coolant and associated containment and pressurization systems. Coolants which do not require pressurizers etc. for high temperature operation have been proposed, such as liquid metals and molten salts, but these coolants lack hydrogen and generally do not yield a thermal neutron spectrum on their own. Therefore, high temperature solid-phase neutron moderators are generally viewed as necessary to enable advanced microreactors.

Solid metal hydrides offer a method of incorporating large quantities of hydrogen into compact nuclear reactor cores without using water. While metal hydrides can be incorporated into compact reactor cores by adding them as separate solid moderator elements between fuel rods, one elegant alternative is to combine the metal hydride solid moderator with the nuclear fuel itself. This means that a thermal neutron spectrum can be achieved merely from the fuel alone, reducing both the size

and weight of the reactor; this was accomplished in the Microreactor Applications Research Validation and EvaLuation (MARVEL) reactor by using stainless steel-clad uranium-zirconium hydride (U-ZrH_x) nuclear fuel, also known as Training, research, isotopes, General Atomics (TRIGA) fuel [1]. However, the use of U-ZrH_x fuel in commercial-scale high temperature reactors is limited by its hydride stability, that is, its ability to retain the hydrogen within the fuel meat. Even after optimization, the hydrogen in U-ZrH_x fuel will dissociate into the gas gap and gradually permeate through the cladding under commercially relevant conditions, eventually leading to a wide variety of undesirable fuel performance and neutronics effects [2]. The inability to retain its hydrogen under high temperatures and burnups for long periods of time limits the applicability of U-ZrH_x for commercial power production. The U-ZrH_x fuel system works well for the MARVEL reactor because, as a demonstration and test reactor, the MARVEL reactor will only be operational intermittently for two years and the maximum burnup and power density are very low compared to commercial designs [3]. However, similar to TRIGA fuel, the operational limits of MARVEL's U-ZrH_x fuel system are determined by high temperature internal gas gap overpressurization leading to hoop stress-induced rupture of the cladding. Since the hydrogen dissociation pressure of δ-ZrH_x increases exponentially with temperature, the contribution of hydrogen gas to the total gas gap pressure is considerable under accident scenario conditions [3, 4].

The primary limitation of U-ZrH_x fuel, which severely limits its maximum allowable operating temperature, power density, and fuel cycle duration, is its ability to retain hydrogen (i.e., prevent it from dissociating into hydrogen gas) at higher, more commercially relevant operating temperatures [2]. Yttrium hydride (without uranium) has been the metal-based high temperature solid moderator of choice since the 1950s because it retains large quantities of hydrogen at higher temperatures than any other known material and is therefore extremely effective at slowing down fast neutrons under commercially relevant nuclear reactor conditions [5-7]. YH_x (where x = H/Y, the atomic ratio of hydrogen to yttrium atoms) is much more stable at high temperatures than ZrH_x; in other words, hydrogen stays bound to yttrium much more readily than zirconium, allowing the material to operate at much higher temperatures for longer periods of time [8]. Designs have been proposed where the YH_x and the U have been separated into bulk geometries for moderator and fuel, respectively, but doing so can result in the YH_x having a positive reactivity coefficient [9]. Therefore, a significant safety feature in U-ZrH_x fuel [10] is lost when the hydride and the uranium are separated.

The hypothetical uranium-yttrium hydride (U-YH_x) fuel concept has been identified as the "ultimate" metal-hydride fuel form since at least the 1970s. Unlike zirconium and uranium [11], however, yttrium and uranium are immiscible (like oil and water) [12]. Historically, attempts have been made to fabricate U-YH_x fuel using a variety of powder-metallurgical techniques, but structural integrity severely degrades under high temperature irradiation due to the seemingly inherent incompatibility between yttrium and uranium, ultimately resulting in the fuel prematurely crumbling [13]. Recent advancements in fabrication methods, however, have succeeded in stabilizing a variety of immiscible binary metals [14, 15], allowing them to remain physically rigid at very high temperatures [16] and under heavy ion irradiation [17, 18]. Experimental efforts for developing a stabilized U-YH_x nuclear fuel for use at high temperatures and burnups are currently underway at the Idaho National Laboratory (INL). While the details of those experiments will be described elsewhere, the objective of this effort is to define key fuel performance properties and relationships of the U-YH_x fuel system with a focus on hydrogen behavior (because hydride stability and hydrogen gas overpressurization are typically limiting parameters for metal hydride fuels). In particular, hydrogen transport through yttrium hydride under the presence of temperature

gradients, known as the Soret effect, is not well understood. To date, the Soret heat of transport of hydrogen in YH_x is typically assumed to be identical to that of hydrogen through ZrH_x due to lack of yttrium hydride data [19, 20]. Forthcoming nuclear fuel performance modeling and simulation studies require a full scope of fuel properties and performance relationships that describe the fuel's behavior, but well-motivated assumptions for the hydrogen behavior in yttrium hydride-based fuel are lacking. Consequently, a sensitivity study of hydride stability to the Soret heat of transport in the hypothetical U-YH_x fuel system during full power steady state operation of a commercial scale sodium-cooled microreactor is of paramount interest.

2. METHODS AND BASE ASSUMPTIONS

The use of high-fidelity computational modeling and simulation tools is paramount to nuclear reactor analyses. During initial scoping studies, however, quick analytical studies can provide a great deal of information without the need for burdensome detailed simulations or computational resources, especially when key gaps of knowledge exist. In this case, we analyze the hydrogen behavior of U-YH_x nuclear fuel under the assumption that advanced fabrication techniques can be used to stabilize the material's microstructure under commercially relevant service conditions; the details of those experiments will be discussed in a forthcoming manuscript. Before any analysis can be performed, we must first establish some microstructural assumptions of the consolidated U-YH_x material upon which behavioral relationships will be based. Due to the similarity between U-YH_x and U-ZrH_x, we assume that the underlying physics of hydrogen behavior in these two fuel systems are similar. In particular, we assume that the microstructure of the U-YH_x fuel is characterized by small metallic uranium inclusions embedded in a yttrium hydride matrix, as is the case for standard U-ZrH_x fuel [3]. This assumption is valid because (a) in practice, the binary metal will be hydrided well above 550 °C such that the yttrium is preferentially hydrided (uranium-hydrogen bonds are not stable above this temperature), and (b) the fuel itself will operate at similarly high temperatures such that uranium-hydrogen bonds are unstable during service [21]. Given this general microstructure, the behavior and motion of the hydrogen in the metal hydride fuel is equivalent to pure YH_x (or ZrH_x for the case of TRIGA fuel) [2, 3, 22, 23]. Exceptions to this behavior include temperature gradients in hydride material cause by the generation of nuclear heat from the uranium inclusions embedded within, as well as possible chemical reactions within the fuel meat caused by the addition of fission products. Both of these topics will be discussed later in the manuscript. The former requires knowledge of the thermophoretic properties of YH_x which are explored in detail in this work.

In order to analyze the hydrogen behavior in U-YH_x, we consider a commercial scale high temperature liquid metal-cooled microreactor which would benefit greatly from the availability of a high temperature self-moderating nuclear fuel. As a test case, we consider a reactor design that uses liquid sodium as the primary coolant, similar to other steel-clad metal hydride-fueled reactor designs [3, 24-27]. The saturated vapor pressure of liquid sodium is very low such that coolant temperatures are limited mostly by creep lifetime characteristics of stainless steel primary system material, typically assumed to be about 550 °C [28]. The fuel pin considered here is similar to TRIGA or MARVEL fuel [3], that is, U-YH_x fuel meat (in place of U-ZrH_x) encapsulated by 304 stainless steel cladding with a helium gas gap in between (in place of air). The geometries and operating conditions assumed in this analysis are shown below in Table 1. This combination of fuel meat composition, power density, and fuel cycle duration equates to a rather high final burnup of about 144 $MWd \cdot kgU^{-1}$; for comparison, typical spent U-ZrH_x TRIGA fuel rods have been measured to reach burnups of at least 36 $MWd \cdot kgU^{-1}$ [29], although the U-ZrH_x fuel system has

demonstrated stability at up to at least 115 MWd·kgU^{-1} [30]. Note that the height of the fuel zone is not discussed here; this is because (a) the vast majority of hydrogen movement through the fuel pin occurs in the radial direction (especially at quasi-steady state), and (b) metal-hydride fuel pins are often designed such that the axial hydrogen flux within the fuel zone is very small in their as-fabricated condition (this will be discussed later in Section 5).

Table 1: Assumed fuel pin design and operating conditions

Property [a]	Value
Initial Fuel Meat Nominal H/Y Ratio, x	1.80 [b]
Fuel Meat Uranium Content, w_U (weight-fraction)	0.30
Enrichment, e (weight-fraction)	0.1975
Fuel Meat Radius, R_{fo} (mm)	6.35
Fuel Meat Power Density, q''' (W·m^{-3})	$1.933 \cdot 10^8$ [c]
Fuel Cycle Duration, t_{irr} (years)	3.5
Mean Coolant Temp. at Cladding Surface, T_m (°C)	550
Gas Gap Thickness, δ_g (μm)	50
Cladding Thickness, t_c (mm)	0.5
Fuel Thermal Conductivity, k_f (W·m^{-1}·K^{-1})	Varies [d]
Gas Gap Conductance, h_g (W·m^{-2}·K^{-1}) [28]	5240 [e]
Cladding Thermal Conductivity, k_c (W·m^{-1}K^{-1}) [31]	23
Coolant Heat Transfer Coefficient, h_{Na} (W·m^{-2}·K^{-1}) [28]	110000

[a] The geometries reported here are representative of their as-fabricated room temperature conditions.
[b] For comparison, the nominal H/Zr ratio in MARVEL fuel is 1.60 with an as-fabricated range of 1.57 – 1.70 [3].
[c] This power density is about 2/3 that of a typical UO_2 pellet in a commercial PWR during full-power operation [28].
[d] The fuel meat thermal conductivity is expected to vary with temperature and will be discussed in Section 3 (see Equation 9).
[e] For conservatism, this value assumes a He gas gap containing a few mol-percent of fission gas [28].

3. CONSTITUTIVE RELATIONSHIPS

The thermophysical properties described in this section are not exhaustive. While a full thermophysical fuel performance analysis will require additional properties and relationships not discussed here, the relationships below are sufficient to perform first-order hydride stability analyses.

3.1 U-YH_x Thermophysical Properties

The composition, atom densities, and mass densities of the components of U-YH_x fuel are given in Equation 1 - Equation 7 below. The uranium weight fraction in the fuel meat can be converted to volume fraction using Equation 8. The fuel composition described in Table 1 corresponds to a fuel meat density of 5.56 g·cm^{-3} and a uranium volume fraction of about 0.088

(less than 9 volume-percent uranium). The atomic fraction of uranium to yttrium, y, is expressed as,

$$y = \frac{N_U}{N_Y} \qquad \text{Equation 1}$$

Where
N_i = atom density of element i (atoms·cm^{-3})

The atomic fraction of hydrogen to yttrium, x, is expressed as,

$$x = \frac{N_H}{N_Y} \qquad \text{Equation 2}$$

The number density of yttrium atoms in the fuel meat, N_Y, is,

$$N_Y = \frac{\rho_{fm} N_A \left(1 - w_U\right)}{M_Y} \qquad \text{Equation 3}$$

Where
ρ_{fm} = fuel meat density (g·cm^{-3})
$N_A = 6.022 \cdot 10^{23}$ = Avogadro's constant (atoms·mol^{-1})
w_U = weight fraction of uranium in the fuel meat
M_Y = 88.906 (g·mol^{-1}) = atomic weight of yttrium

The atomic fraction of uranium to yttrium atoms in the fuel meat can also be expressed as,

$$y = \frac{M_Y}{M_U} \cdot \frac{w_U}{1 - w_U} \qquad \text{Equation 4}$$

Where
$M_U = 235e + 238\left(1 - e\right)$ = the atomic weight of uranium (g·mol^{-1})
e = uranium enrichment

The density of the yttrium hydride phase in the fuel meat is given by,

$$\rho_{YH_x} = 4.37 - x \cdot 5.82 \cdot 10^{-2} \qquad \text{Equation 5}$$

Where
ρ_{YH_x} = density of the YH_x phase at room temperature (g·cm^{-3}) [32]

The density of the fuel meat is expressed as,

$$\rho_{fm} = \left(\frac{w_U}{\rho_U^0} + \frac{1 - w_U}{\rho_{YH_x}} \right)^{-1} \qquad \text{Equation 6}$$

Where
ρ_{fm} = U-YH_x fuel meat density (g·cm^{-3})
ρ_U^0 = 19.05 (g·cm^{-3}) = maximum theoretical density of uranium at room temperature [33]

The density of the uranium in the fuel meat is given by,

$$\rho_U = w_U \rho_{fm}$$ Equation 7

Where
ρ_U = uranium density of the fuel ($g \cdot cm^{-3}$)

The volume fraction of uranium in the fuel meat is expressed as,

$$V_U = \frac{w_U \rho_{fm}}{\rho_{U_0}}$$ Equation 8

Where
V_U = volume fraction of uranium in the U-YH_x fuel meat

There is some uncertainty in the thermal conductivity of the proposed U-YH_x fuel system; however, this property will be determined experimentally in future work. For now, however, we believe that the likely thermal conductivity behavior of the stabilized U-YH_x fuel meat will be as follows. While a simple rule-of-mixing approach is a mathematically simple way of approximating the effective thermal conductivity (ETC) of a binary composite, it is often not an accurate prediction of composite heat transfer behavior. Unlike many other thermophysical properties (density, specific heat, etc.), the thermal conductivity of composite materials may not be well-approximated by a simple linear rule-of-mixing because the effective thermal conductivity of a material is path-dependent and not mass or volume-dependent. Until experimental thermal conductivity data becomes available, the thermal conductivity shall be approximated using the Maxwell model as described in [34], shown in Equation 9. The thermal conductivities of uranium [33] and δ-YH_x [6] are given in Equation 10 and Equation 11, respectively. Note that the thermal conductivity of δ-YH_x is not well understood at high temperatures; however, this property does appear to decrease approximately linearly at temperatures above 573 K [35]. It is also unclear how variations in H/Y ratio influence the metal-hydride's thermal conductivity at high temperatures. We therefore assume that the thermal conductivity of δ-YH_x is insensitive to small variations in hydrogen content and decreases linearly with increasing temperature, where this relationship is extrapolated beyond 773 K in Equation 11 up to a phase transition occurring at ~1600 K (*vide infra*).

$$k_f = k_{YH} \frac{k_U + 2k_{YH} + 2\left(k_U - k_{YH}\right)V_U}{k_U + 2k_{YH} - \left(k_U - k_{YH}\right)V_U}$$ Equation 9

Where
k_f = effective thermal conductivity of the U-YH_x composite fuel meat ($W \cdot m^{-1} \cdot K^{-1}$) [34]
k_U = thermal conductivity of metallic uranium ($W \cdot m^{-1} \cdot K^{-1}$), see Equation 10
k_{YH} = thermal conductivity of δ-YH_x ($W \cdot m^{-1} \cdot K^{-1}$), see Equation 11
$V_U \in (0, 0.25)$ = uranium volume fraction in the fuel meat, see Equation 8

$$k_U = 22 + 0.023\left(T_K - 273\right)$$ Equation 10

Where
k_U = thermal conductivity of uranium ($W \cdot m^{-1} \cdot K^{-1}$) [33]
$T_K \in (293, 1405)$ = temperature (K)

$$k_{YH} = \begin{cases} T_K^{\,2} \cdot 1.4229 \cdot 10^{-4} - T_K \cdot 0.22641 + 128 & 293 \le T_K < 573 \\ -0.03076 \cdot T_K + 63.03 & T_K \ge 573 \end{cases} \quad \text{Equation 11}$$

Where
k_{YH} = thermal conductivity of δ-YH ($W \cdot m^{-1} \cdot K^{-1}$) [6]
$T_K \in (373, 1600)$ = temperature (K)

Four major assumptions of the Maxwell model of thermal conductivity are that (a) the dispersant phase (uranium) and the matrix phase (yttrium hydride) are non-interacting, (b) the dispersant volume fraction is less than about 0.25, (c) the dispersant is randomly distributed as spherical inclusions throughout the matrix, and (d) the composite is very close to zero porosity. We anticipate these four assumptions to be true for the stabilized U-YH_x, but it is currently unclear how microstructural features associated with the manufacturing method might impact the consolidated fuel's ETC. This will be investigated experimentally and discussed in a forthcoming manuscript. The thermal conductivity relationships for uranium, yttrium hydride, and the consolidated fuel meat composite are shown in Figure 1. Also shown for comparison is the thermal conductivity of U-$ZrH_{1.6}$ nuclear fuel, which is approximately 18 $W \cdot m^{-1} \cdot K^{-1}$ and remains constant over a large temperature range [36, 37].

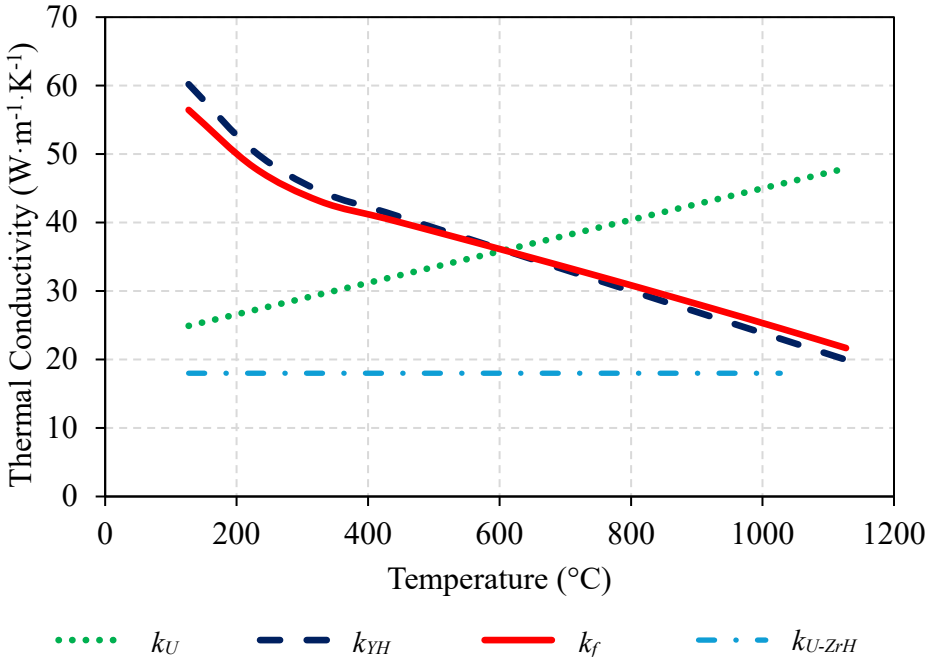

Figure 1: Thermal conductivities vs. temperature of uranium (green dotted line), δ-YH_x (blue dashed line), and U-YH_x whose composition is defined in Table 1 (red solid line) according to Equation 10, Equation 11, and Equation 9, respectively. The thermal conductivity of standard U-ZrH fuel is also shown (blue dash-dot) for comparison.

3.2 Hydrogen Behavior

The attractive aspect of the proposed U-YH_x fuel system is its ability to contain large quantities of hydrogen within the fuel meat itself while operating at high temperatures. In this regard, more hydrogen is preferred in order to yield more neutron moderation within the fuel

volume. However, the material is expected to be above 600 °C during service, and stoichiometries where $x > 2.0$ are susceptible to exponentially excessive hydrogen dissociation as temperature increases. While this study considers a nominal H/Y of 1.80 (see Table 1), the pure face-centered cubic δ-phase of YH_x is stable over a wide composition range under relevant service conditions as shown in Figure 2 [38].

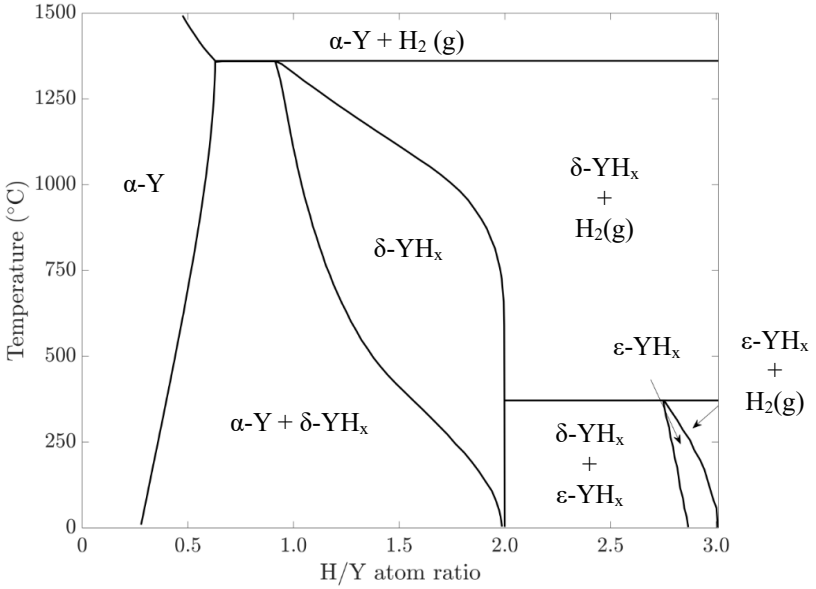

Figure 2: The yttrium-hydrogen phase diagram, redrawn from [38].

Hydrogen in metal-hydrides is mobile. The hydrogen flux through the fuel meat is a combination of Fickian diffusion (due to hydrogen composition gradients), Soret diffusion (due to temperature gradients), and stress diffusion (due to stress gradients). The current analysis assumes that the stresses within the fuel during full power steady state operation are sufficiently small that hydrogen diffusion due to stress gradients can be ignored with negligible error, as is commonly done for U-ZrH_x fuel [39]. Ignoring axial hydrogen redistribution (this assumption will be supported later in Section 5), the radial hydrogen flux through the U-YH_x fuel meat is given by Equation 12 [3].

$$J_H = J_{Fick} + J_{Soret} + J_{Stress}$$

$$J_H = -D_s \nabla C_H - \frac{D_s C_H Q}{RT^2} \nabla T + \frac{D_s C_H V_H}{RT} \nabla \sigma_H$$

$$\therefore$$

$$J_H(r) \approx -D_s \frac{\rho_Y}{M_Y} \left(\frac{dx(r)}{dr} + \frac{T_Q}{T_K(r)} \frac{x(r)}{T_K(r)} \frac{dT_K(r)}{dr} \right) \qquad \text{Equation 12}$$

Where
r = radius (m)
$J_H(r)$ = hydrogen flux as a function of radius in the fuel pellet ($x(r) \cdot m^{-2} \cdot s^{-1}$)
J_{Fick} = Fickian diffusion flux

J_{Soret} = Soret thermal diffusion flux
J_{Stress} = stress diffusion flux ≈ 0
D_s = diffusion coefficient of hydrogen in the hydride ($m^2 \cdot s^{-1}$), see Equation 13
C_H = hydrogen concentration in YH_x solid solution
R = universal gas constant
Q = heat of transport of hydrogen in YH_x
V_H = partial molar volume of hydrogen in YH_x
σ_H = hydrostatic stress
ρ_Y = mass-density of yttrium ($kg \cdot m^{-3}$)
M_Y = atomic weight of Y ($kg \cdot mol^{-1}$)
$x(r)$ = H/Y ratio as a function of radius in the fuel pellet
T_Q = heat of transport temperature of H in U-YH_x (K)
$T_K(r)$ = radial temperature profile in the fuel meat (K)

The hydrogen content in Equation 12 is written in terms of the hydrogen-to-yttrium atomic ratio in the fuel, x, in order to quickly assess the composition and crystallographic phase of the material as a function of position within the fuel meat. The Fickian diffusion coefficient of hydrogen in δ-YH_x, D_s, is given by Equation 13 [40]. The Soret heat of transport, Q, has never been experimentally measured [20]. Consequently, when modeling hydrogen transport in metal hydrides due to the Soret effect, the heat of transport of H in YH_x is often assumed to be equal to that of ZrH_x [19]. Dividing the heat of transport by the universal gas constant yields a quantity that has units of temperature, $Q/R = T_Q$; this quantity is referred to as the Soret heat of transport temperature, and it is equal to T_Q = 640 K for U-ZrH_x fuel [23]. Assuming that the hydrogen in U-YH_x migrates from hot to cold regions within the solid, like in U-ZrH_x, this means that T_Q is greater than zero; however, the true value of T_Q in U-YH_x and U-ZrH_x may be different.

$$D_s = D_0 e^{\left(\frac{-E_a}{RT_K}\right)} \qquad \text{Equation 13}$$

Where
D_s = Fickian diffusion coefficient of hydrogen in δ-YH_x [40]
$D_0 = 3.1 \cdot 10^{-8}$ ($m^2 \cdot s^{-1}$)
E_a = activation energy = 41,200 ($J \cdot mol^{-1}$)
R = universal gas constant = 8.314 ($J \cdot mol^{-1} \cdot K^{-1}$)
T_K = temperature (K)

Assuming that the plenum and gas gap volume is sufficiently small that the loss of hydrogen due to hydrogen dissociation (in the gas gap, before permeation and escape through the cladding) is negligible under steady state operating conditions [3], the steady state solution to Equation 12 is given by Equation 14 below. The integration constant in Equation 14, A, can be determined by plugging Equation 14 into Equation 15. This requires knowledge of the average H/Y ratio, the Soret heat of transport temperature, and the fuel meat temperature profile. To a first order approximation, the time it takes for radial thermal diffusion and hydrogen redistribution to occur can be approximated using Equation 16 which also depends on the value of T_Q (because the temperature gradient is the driving force for redistribution) [3]. Note from inspection of Equation 14 and Figure 2 that phase stability of the fuel meat after hydrogen has redistributed under a temperature gradient cannot be determined without knowledge of T_Q.

$$x(r) = Ae^{T_Q / T_K(r)}$$ Equation 14

Where
r = radius (cm)
$x(r)$ = H/Zr ratio as a function of radius in the cylindrical fuel pellet
A = integration constant
T_Q = heat of transport temperature of H in YH_x (K)
$T_K(r)$ = radial temperature profile in the fuel meat (K)

$$x_{avg} = \frac{2}{R_{fo}^{\ 2}} \int_0^{R_{fo}} r \cdot x(r) dr$$ Equation 15

Where
x_{avg} = average H/Y ratio in the fuel pellet
r = radius (cm)
R_{fo} = U-YH_x fuel meat outer radius (cm)

$$t_{radial} \approx \frac{\pi R_{fo}^{\ 2}}{2D_s} \cdot \frac{T_Q}{T_{CL} - T_{fo}}$$ Equation 16

Where
t_{radial} = duration of time for thermally driven hydrogen redistribution to occur radially (s)
D_S = diffusion coefficient of hydrogen in the fuel ($m^2 \cdot s^{-1}$)
R_{fo} = outer radius of the fuel meat (m)
T_Q = heat of transport temperature of H in YH_x

The hydrogen in metal hydrides increasingly dissociates into hydrogen gas as both temperature and hydrogen concentration in the solid increase. In general, if the metal hydride is contained within a sealed vessel, some hydrogen dissociates out of the solid to occupy the internal vessel space as hydrogen gas (increasing the gas pressure in the vessel), while some gas-phase hydrogen recombines with the solid (decreasing the gas pressure in the vessel). For a given material, the hydrogen dissociation equilibria are defined by the pressure and temperature at which the rate of hydrogen transferring from gas-to-solid and solid-to-gas are equal, yielding a thermodynamic steady state. These relationships are important for metal hydride nuclear fuels because when dissociated hydrogen gas enters the gas gap, (a) the hydrogen gradually leaks through the cladding, thereby reducing the hydrogen overpressure, which promotes further desorption from the fuel pin, and (b) hydrogen gas in the gas gap exacerbates internal gas overpressurization and possible stress-rupture of the cladding during a high temperature excursion. High temperature hydrogen dissociation isochores specific to yttrium hydride are available in the literature. In this work, data has been taken from [41] to generate the relationship shown in Equation 17; the parameters B and d were empirically determined with statistical coefficients of determination of $R^2 > 99.99\%$ from the mean values reported in [41]. Note that the hydrogen

pressure is expressed here in units of Torr, and it is assumed to be appropriate for any combination of temperature and hydrogen concentration so long as the yttrium hydride is in the δ phase (see Figure 2). Also note that the hydrogen dissociation pressure here is dependent upon the H/Y ratio at the solid-gas interface (as opposed to the average x value) which, because of the Soret effect, will always be higher at the pellet surface than in the bulk.

$$P_{\delta-YH_x} = e^{2.303B-\frac{d}{T_K}} \qquad \text{Equation 17}$$

Where

$P_{\delta-YH_x}$ = equilibrium partial pressure of hydrogen gas for δ-phase YH_x (Torr)

T_K = metal-hydride temperature at the solid-gas interface (K)

$x \in (1.2, 2.0)$ = H/Y ratio at the solid-gas interface

$$B = 255.128 \cdot x^5 - 1898.266 \cdot x^4 + 5617.835 \cdot x^3 - 8264.63 \cdot x^2 + 6046.559 \cdot x - 1750.929$$

$$d = 6.421827 \cdot 10^5 \cdot x^5 - 4.788489 \cdot 10^6 \cdot x^4 + 1.41948 \cdot 10^7 \cdot x^3 - 2.090897 \cdot 10^7 \cdot x^2 + 1.531054 \cdot 10^7 \cdot x - 4.435128 \cdot 10^6$$

The parameters B and d are plotted in Figure 3 for comparison between the curve fit and experimentally measured data. The resulting equilibrium hydrogen dissociation pressure vs. temperature is shown in Figure 4. Also shown in Figure 4 is the equilibrium hydrogen dissociation pressure of $ZrH_{1.60}$, which is the nominal hydrogen content reported for standard TRIGA fuel. Note that even though the hydrogen content in $YH_{1.80}$ is much larger, the equilibrium hydrogen dissociation pressure is several orders of magnitude lower than for $ZrH_{1.60}$.

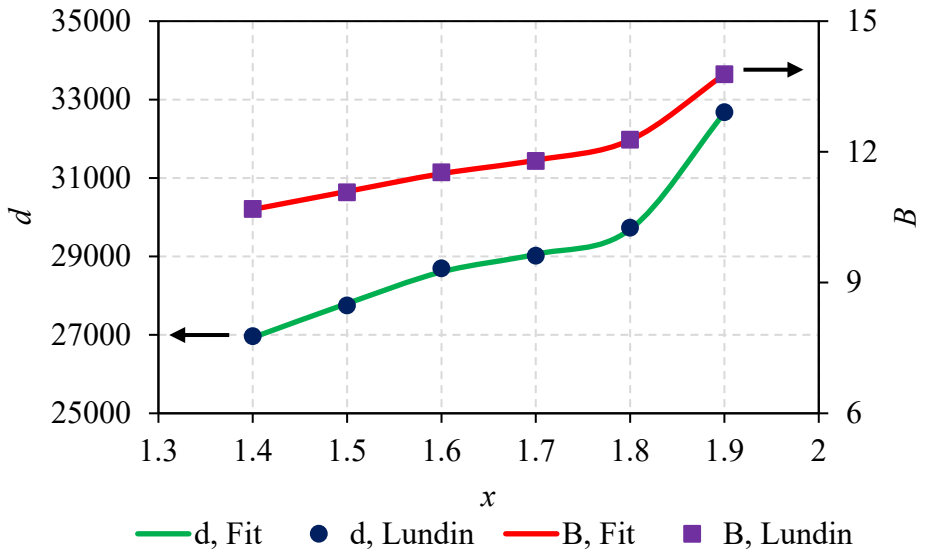

Figure 3: Plot of B and d values for YH_x according to measured literature mean values (Lundin [41]) vs. the curve fit (Equation 17).

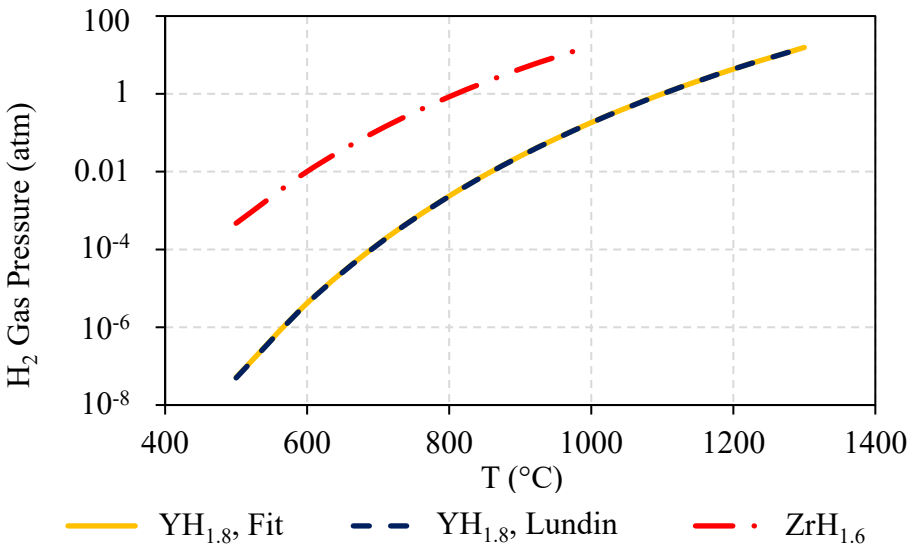

Figure 4: Equilibrium hydrogen dissociation pressure for δ-$YH_{1.80}$ according to the curve fit (solid yellow line, see Equation 17) vs. measured data (blue dashed line [41]). Also included is the equilibrium hydrogen dissociation pressure for δ-$ZrH_{1.60}$ (red dash-dot [4]) for comparison.

Hydrogen gas that has dissociated out of the fuel meat and into the gas gap will gradually permeate through the cladding and into the coolant. Hydrogen that leaks through the cladding is normally assumed to be unrecoverable from the fuel zone. Consequently, unlike hydrogen redistribution, hydrogen leakage through the cladding acts to gradually decrease the bulk hydrogen content in the fuel meat over time. When the temperature drop through the cladding is small (a few degrees K in this case), the hydrogen flux through the cladding is dependent upon (a) the hydrogen partial pressure in the gas gap, (b) the temperature of the cladding, and (c) the thickness of the cladding as defined by Sievert's law in Equation 18. The hydrogen permeability through 304 stainless steel is given by Equation 19 [22, 42].

$$J_H(T_K) = \Phi(T_K)\frac{\sqrt{P}}{t_c} \qquad \text{Equation 18}$$

Where

J_H = hydrogen flux through the steel ($mol \cdot m^{-2} \cdot s^{-1}$)

$\Phi(T_K)$ = hydrogen permeability in the cladding $\left(\frac{mol\ H_2}{m \cdot s \cdot \sqrt{Pa}}\right)$

P = hydrogen gas pressure in the gas gap (Pa), see Equation 17

t_c = cladding thickness (m)

$$\Phi(T_K) = \Phi_0 e^{-6760/T_K} \qquad \text{Equation 19}$$

Where

$\Phi(T_K)$ = hydrogen permeability in 304 SS $\left(\frac{mol\ H_2}{m \cdot s \cdot \sqrt{Pa}}\right)$

$$\Phi_0 = 5.4 \cdot 10^{-8} \left(\frac{mol\, H_2}{m \cdot s \cdot \sqrt{Pa}} \right)$$

T_K = temperature (K)

The decrement of the average H/Y ratio in the fuel meat due to hydrogen escape through the cladding is related to the hydrogen flux through the cladding by Equation 20 [22]. The hydrogen flux through the cladding is a time-dependent quantity even under steady state reactor operation because the hydrogen pressure in the gas gap will change as the fuel meat's hydride stoichiometry changes. High fidelity computational fuel performance modeling and simulation codes, such as Idaho National Laboratory's BISON, exist which can account for such time dependent variations by performing numerical iterations over sufficiently small time steps [43]. This is a burdensome task to perform analytically; however, note that performing this calculation using even one single time step yields ever-smaller error as the decrease in total hydrogen content in the fuel meat (Equation 20) decreases, enabling a quick analytical calculation to yield conservative yet reasonable first-order approximation results [2].

$$\frac{d\left(x_t / x_0\right)}{dt} = \frac{-J_H\left(T_K\right)}{N_{H,0} d} \qquad \text{Equation 20}$$

Where
x_0 = H/Y ratio in the fuel at time step i
x_t = H/Y ratio in the fuel at timestep $i + 1$
J_H = hydrogen flux through the cladding (mol·m^{-2}·s^{-1})
$N_{H,0}$ = hydrogen density in the fuel at time step i (mol·m^{-3}), see Equation 2
d = inner diameter of the cladding (m)

3.3 Thermal Gradients

The temperature limits of standard TRIGA and MARVEL fuel are defined by the fuel meat temperature [3, 23]. While the temperature profile in nuclear fuel pins is important for any type of fuel, it is arguably even more important for metal hydride fuel due to the unavoidable phenomena of hydrogen redistribution and dissociation. The radial temperature profile within the fuel pin is given by Equation 21 (axial effects will be discussed later in Section 5). Note from Equation 9 that the thermal conductivity of the U-YH_x fuel meat is expected to also vary with temperature. Analytically, this can be resolved by obtaining the average thermal conductivity in the fuel meat using Equation 22. The radial temperature profile in the cylindrical U-YH_x fuel meat is therefore expressed analytically by Equation 23. In reality, many of the variables used in Equation 21 and Equation 22 can change over time due to cracks, agglomerations of fission gases/pores, thermal expansion, radiation-enhanced swelling, etc., but changes in the fuel meat temperature profile caused by these evolving effects are ignored for this preliminary scoping study.

$$T_{CL} = \pi R_{fo}{}^2 q''' \left[\frac{1}{4\pi \left\langle k_f \right\rangle} + \frac{1}{2\pi R_g h_g} + \frac{1}{2\pi k_c} \ln\left(\frac{R_{co}}{R_{ci}} \right) + \frac{1}{2\pi R_{co} h} \right] + T_m \qquad \text{Equation 21}$$

Where

T_{CL} = fuel meat centerline temperature (K)

T_m = mean coolant temperature at cladding interface (K)
R_{fo} = fuel meat outer radius (m)
$R_g = \left(R_{fo} + R_{ci}\right)/2$ = average gas gap radius (m)
R_{ci} = cladding inner radius (m)
R_{co} = cladding outer radius (m)
q''' = fuel meat volumetric heat generation rate in the fuel meat ($W \cdot m^{-3}$)
$\left\langle k_f \right\rangle$ = fuel meat average thermal conductivity ($W \cdot m^{-1} \cdot K^{-1}$), see Equation 22
h_g = gas gap conductance ($W \cdot m^{-2} \cdot K^{-1}$)
k_c = cladding thermal conductivity ($W \cdot m^{-1} \cdot K^{-1}$)
h_{Na} = coolant heat transfer coefficient ($W \cdot m^{-2} \cdot K^{-1}$)

$$\left\langle k_f \right\rangle = \frac{\int_{T_{fo}}^{T_{CL}} k_f(T)\,dT}{T_{CL} - T_{fo}} \qquad \text{Equation 22}$$

Where
$\left\langle k_f \right\rangle$ = fuel meat average thermal conductivity ($W \cdot m^{-1} \cdot K^{-1}$)
k_f = temperature-dependent thermal conductivity of the fuel meat ($W \cdot m^{-1} \cdot K^{-1}$)
T_{CL} = fuel meat centerline temperature (K)
T_{fo} = fuel meat outer surface temperature (K)

$$T_K(r) = T_{fo} + \left(T_{CL} - T_{fo}\right)\left[1 - \left(\frac{r}{R_{fo}}\right)^2\right] \qquad \text{Equation 23}$$

Where
$T_K(r)$ = fuel temperature (K) at radial position r
r = radial position (m) in the cylindrical fuel pellet, $0 \le r \le R_{fo}$
R_{fo} = fuel meat outer radius (m)
T_{CL} = fuel meat centerline temperature (K)
T_{fo} = temperature at the fuel meat radial surface (K)

4. RESULTS

4.1 Radial Thermal Profile

Using Equation 21, the average cladding temperature is about 561 °C and varies only a few degrees from the hot (inner) surface to the cold (outer) surface. Despite being mostly helium, the gas gap is the main source of thermal resistance in the fuel pin, as to be expected [2]. Using Equation 21 - Equation 23, the temperature profile in the fuel meat varies strongly with radius as shown in Figure 5. In reality, the temperature profile will change slightly over time not only due to dimensional changes in the fuel pin, but also because of changes in gas gap composition as fission gases are released from the solid fuel matrix. Figure 5 reveals a large radial temperature

gradient in the fuel meat of about 60 °C for the fuel described in Table 1 (about 9 °C·mm^{-1}). This temperature gradient is large despite the fuel's large thermal conductivity because the power density in the fuel meat is large under these conditions. Experimental studies suggest that δ-YH_x appears to remain stable under irradiation at these temperatures [44].

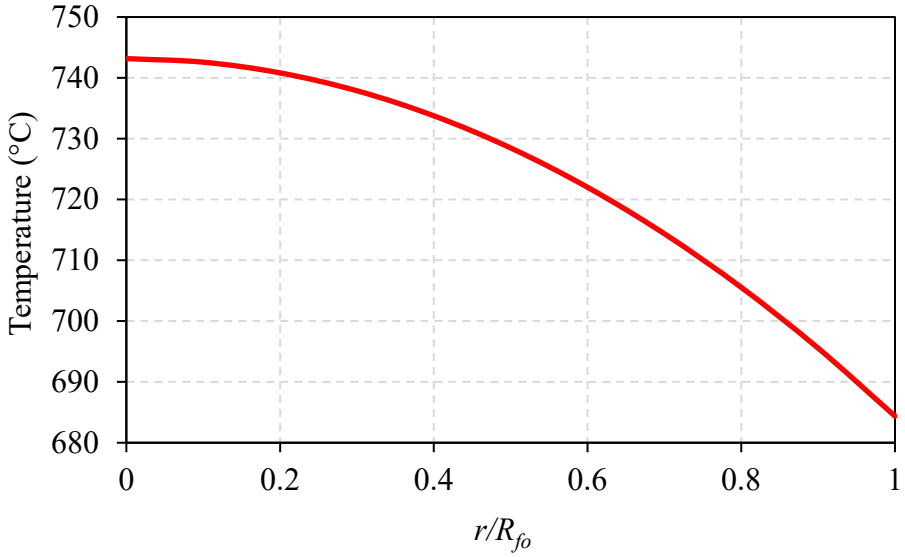

Figure 5: Radial temperature profile in the U-YH_x fuel meat described by Table 1, calculated using Equation 21 - Equation 23.

4.2 Hydrogen Redistribution Behavior vs. T_Q

In the fresh fuel configuration, the hydrogen content is assumed to be approximately homogeneous throughout the fuel pellet radius. Imposing the temperature gradient shown in Figure 5 will cause the hydrogen to redistribute radially until the equilibrium redistribution profile is reached according to Equation 14. This relationship varies with T_Q as shown in Figure 6. The time it takes for the radial hydrogen composition profile to reach steady state can be approximated using Equation 16 which is also dependent upon the value of T_Q as shown in Figure 7. The heat of transport temperature for U-ZrH_x fuel, T_Q = 640 K, is shown in both Figure 6 and Figure 7 in red. Note that the time it would take for U-YH_x fuel to reach equilibrium would be different than in U-ZrH_x fuel even if T_Q were 640 K and the operating conditions and geometries were the same for both because (a) the two materials have different thermal conductivities k_f and (b) the two materials have different diffusion coefficients D_s. From Figure 6, we see that the redistributed value of H/Y at the fuel-gas interface, $x(R_{fo})$, varies by up to about 0.039 (about 2%) over the heat of transport temperature range of $300 \leq T_Q \leq 1000$ K. Figure 7 shows that the time it takes for radial hydrogen redistribution to reach equilibrium takes between about two weeks to two months depending on the value of T_Q. Regardless, this radial redistribution time is relatively small compared to multi-year fuel cycle durations.

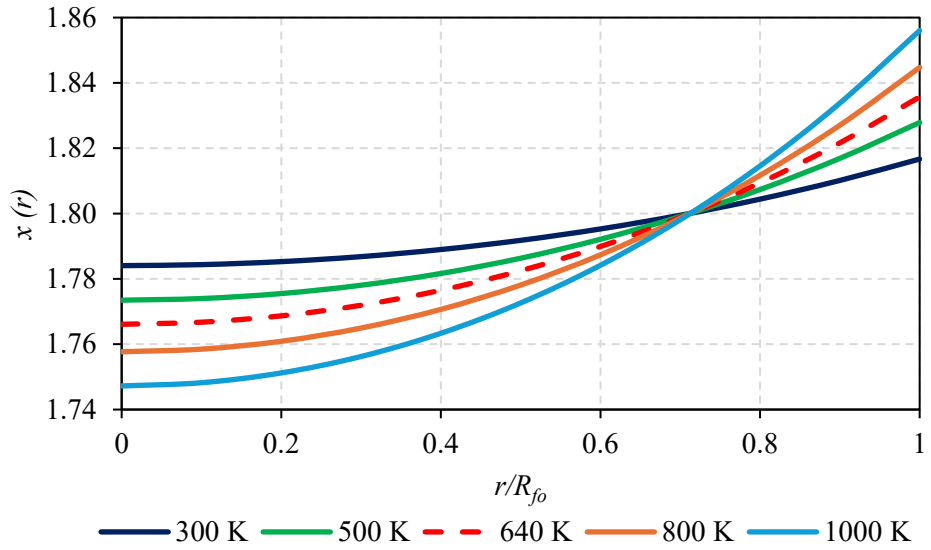

Figure 6: Radial equilibrium hydrogen redistribution profile vs. T_Q in U-YH_x fuel (see Table 1) under the temperature gradient shown in Figure 5, calculated using Equation 14. The dotted red line represents the heat of transport temperature for U-ZrH_x fuel, T_Q = 640 K.

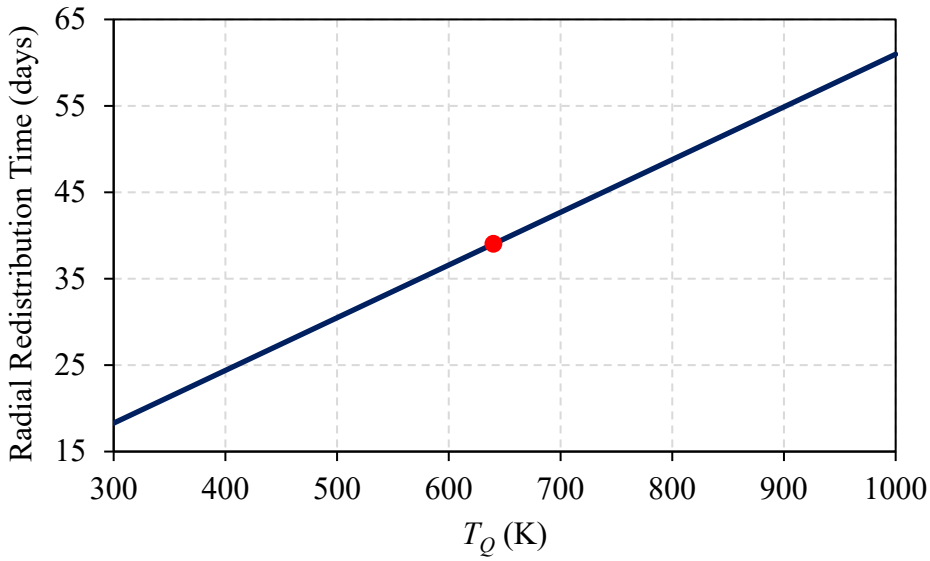

Figure 7: Approximated time to reach radial redistribution equilibrium (see Figure 6) vs. T_Q in U-YH_x fuel (see Table 1) under the imposed temperature gradient shown in Figure 5, calculated using Equation 16. The red dot represents the heat of transport temperature for U-ZrH_x fuel, T_Q = 640 K.

4.3 Hydrogen Gas Pressure and Leakage Rate vs. T_Q

While Figure 6 shows that the equilibrium hydrogen concentration at the fuel meat surface only varies by up to 2% for T_Q values ranging from 300 K to 1000 K, the relationships describing hydrogen dissociation are non-linear with composition which directly impacts the hydrogen

dissociation pressure and hydrogen leakage rate through the cladding (Equation 20). The equilibrium hydrogen dissociation pressure vs. T_Q for the U-YH_x fuel described in Table 1 is calculated using Equation 17 and illustrated in Figure 8. The initial hydrogen leakage rate through the steel cladding (i.e. when radial hydrogen redistribution has reached equilibrium but before the fuel meat has lost an appreciable amount of hydrogen due to leakage) is calculated using Equation 20 and is shown in Figure 9. The equilibrium hydrogen dissociation pressure vs. T_Q and hydrogen leakage rate through the cladding vs. T_Q are both linear. Note that while varying the value of T_Q results in only a small difference in H/Y ratio at the fuel-gas interface (Figure 6), the resulting dissociation pressure and hydrogen leakage rate vary by up to about 16% and 8%, respectively.

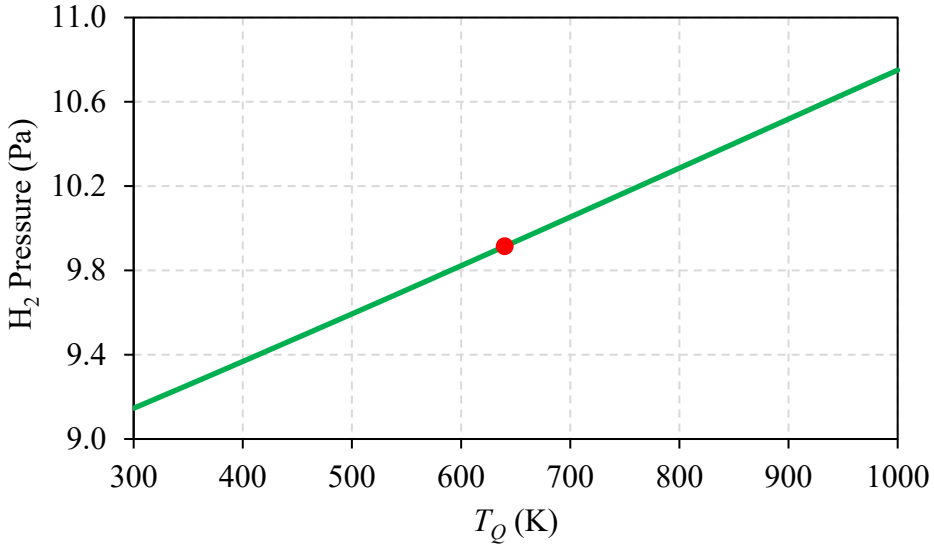

Figure 8: Equilibrium hydrogen dissociation pressure vs. T_Q in U-YH_x (see Table 1) early in the fuel's operational cycle, calculated using Equation 17. The red dot represents the heat of transport temperature for U-ZrH_x fuel, T_Q = 640 K.

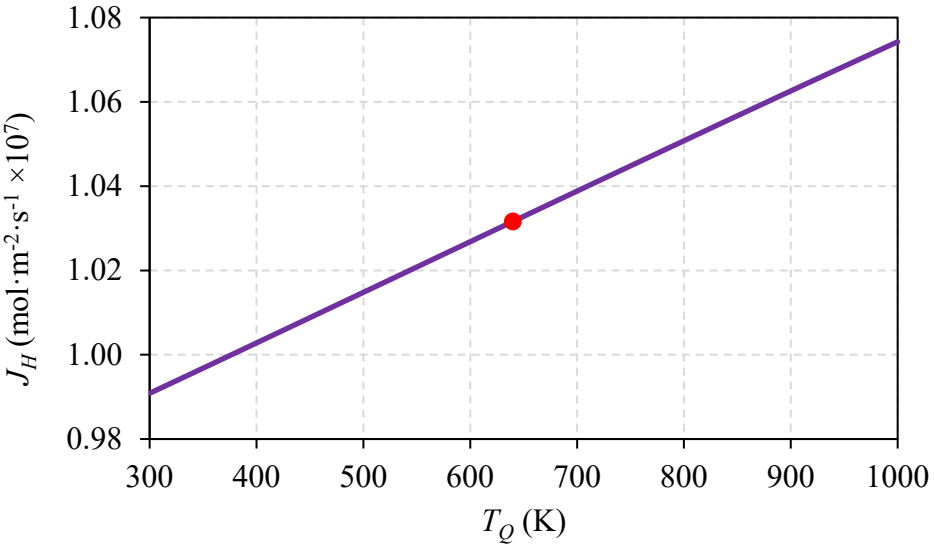

Figure 9: Hydrogen leakage rate through the steel cladding vs. T_Q in U-YH_x (see Table 1) early in the fuel's cycle operational cycle, calculated using Equation 20. The red dot represents the heat of transport temperature for U-ZrH_x fuel, T_Q = 640 K.

4.4 Hydride Evolution vs. T_Q

From Figure 6, the radial hydrogen redistribution profile varies up to only Δx of 0.039 at the fuel meat surface under the conditions considered here over the range of T_Q from 300 K to 1000 K. This variation in surface hydrogen content due to uncertainty in the value of T_Q is probably comparable or smaller to the variations in hydrogen content found in real commercial metal hydride fuel; while materials are fabricated with the aim of attaining as-designed nominal values (where x = 1.80 has been chosen in this study), the true values will vary in practice even in the as-fabricated condition. This indicates that the radial hydrogen redistribution profile in U-YH_x fuel is relatively insensitive to the assumed value of T_Q. However, since hydrogen dissociation and therefore hydrogen leakage increase exponentially with hydrogen composition, Figure 8 and Figure 9 show that these two parameters vary by up to 16% and 8%, respectively, when T_Q is varied from 300 K to 1000 K. When considering steady state reactor operation, however, two important concerns regarding hydrogen behavior in this fuel system are: (1) does uncertainty in the value of T_Q significantly impact our ability to predict neutronics properties of the system, and (2) does uncertainty in the value of T_Q significantly impact our ability to predict δ-phase stability in the fuel? Both questions can be informed by a quick analytical calculation using Equation 20. If the calculation is performed using one single time step, which is to say that the hydrogen pressure in Equation 20 remains constant over the full 3.5 year operational fuel cycle, then the average H/Y ratio in the fuel meat at end-of-life (EOL) has decreased by some value which is also dependent upon T_Q. This dependence is shown in Figure 10 which reveals that the variation in x_{avg} at EOL vs. T_Q is very small, only up to 0.05% between T_Q of 300 K to 1000 K. This analysis suggests that items (1) and (2) above are insensitive to the assumed value of T_Q under the full power steady state operating conditions assumed here. Note that this "single timestep" method slightly overestimates the rate at which hydrogen leakage occurs over time because hydrogen pressure in the gas gap decreases as the hydrogen content in the fuel decreases.

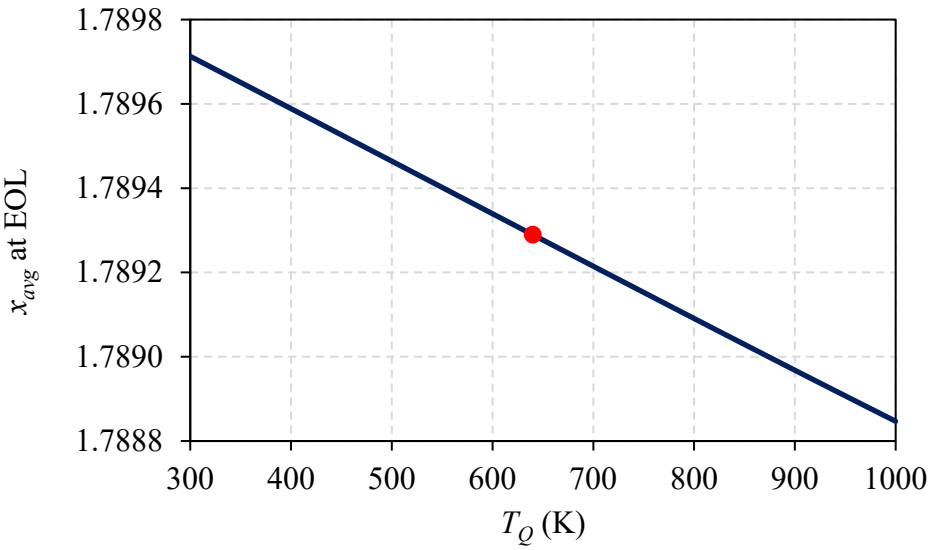

Figure 10: Average H/Y ratio in the fuel meat at EOL (3.5 years at full power, see Table 1) vs. T_Q. This data was calculated using Equation 20 with one single time step. The red dot represents the heat of transport temperature for U-ZrH_x fuel, T_Q = 640 K.

5. DISCUSSION

The following discussions are generally qualitative for illustrative purposes only, but it is important in order to design a metal hydride fuel for extreme conditions. Consequently, although calculations are not performed below for operating conditions in any specific reactor design, relevant equations are provided for clarity.

5.1 Discussion of Results

YH_x holds onto its hydrogen so strongly that even under the extreme conditions and large temperature gradients representative of a commercially relevant liquid metal-cooled nuclear reactor, the H/Y ratio in the U-YH_x fuel over the course of a complete operational fuel cycle is insensitive to the assumed value of T_Q. This might not be true for accident scenarios where temperatures are much higher. The cladding material chosen in this analysis is austenitic stainless steel because it is used in U-ZrH_x fuel and is stable in molten sodium [3]. Austenitic stainless steels, however, rapidly lose strength above about 600 °C, down to a tensile strength of only tens of MPa at 1000 °C [3]. Understanding the sensitivity of T_Q to the true operational limits of this fuel pin would require more information from the thermal hydraulics design of the reactor under consideration, as well as the conditions of the accident scenarios of interest; however, one can conclude qualitatively that as fuel temperatures increase for a given accident scenario, the role of T_Q is becomes more important in understanding the fuel pin's internal gas overpressurization limits regardless of which cladding material is selected.

5.2 Axial Effects in Hydride Fuels

Discussion of axial temperature gradients has deliberately been omitted from the analysis up to this point. Strictly speaking, hydrogen will redistribute axially throughout the fuel pin, both

by axial Soret transport through the solid fuel meat and by portions of the fuel meat outer surface preferentially absorbing hydrogen gas where the isochore is favorable to do so. Under axial temperature gradients found in any nuclear reactor core, one would expect axial hydrogen redistribution within a metal hydride fuel element to eventually be noticeable if the hydrogen content were homogeneous throughout the height of the fuel pin in the fresh fuel configuration. Even in modest hydride-fueled research reactors, however, designing the fuel pin in this manner is known to exacerbate a variety of undesirable phenomena such as power distribution anomalies, excessive fuel meat cracking, hydride swelling-exacerbated fuel-cladding mechanical interactions, and so on [45]. The hydrogen in any metal hydride fuel should ideally move around as little as possible. In practice, this is accomplished in real metal hydride fuel pins, in part, by designing the fuel pin with an as-fabricated axial composition gradient to counteract the axial temperature profile from the beginning of the fuel cycle. As an example, while the nominal H/Zr value in MARVEL fuel is reported to be x_{nom} = 1.60, MARVEL's as-fabricated fuel meat average hydrogen content is lowest (H/Zr within 1.57 – 1.60) near the center of the fuel pin where the temperature will be the highest during operation, while the top and bottom fuel pellets have much higher hydrogen content (up to x_{avg} = 1.70) where the fuel will be the coldest [3]. Designing metal hydride fuel rods in this manner enables the hydrogen dissociation pressure at the fuel meat surface to vary far less throughout the height of the rod from the start (though some small axial variations are unavoidable in practice).

The fuel designer should consider (a) the expected axial temperature profile of the fuel meat outer surface and (b) a fuel meat composition profile to offset the axial temperature profile in order to minimize axial hydrogen migration during service. Ignoring axial heterogeneities (thermal expansion, swelling, etc.), and assuming single-phase coolant, force coolant flow, and a "chopped cosine" axial power profile in the fuel zone, the axial temperature profile of the fuel meat surface can be approximated using Equation 24.

$$T_{fo}(z) = q'(z) \cdot \left[\frac{1}{2\pi R_g h_g} + \frac{1}{2\pi k_c} \ln\left(\frac{R_{co}}{R_{ci}} \right) + \frac{1}{2\pi R_{co} h_{Na}} \right] + T_m(z) \qquad \text{Equation 24}$$

Where

$T_{fo}(z)$ = axial temperature profile of the fuel meat outer surface (K)

$z \in (-H/2, H/2)$ = fuel zone height (m), where $z = 0$ is the mid-plane, halfway up the fuel zone

$q'(z)$ = linear heat generation rate axial profile ($W \cdot m^{-1}$)

$$q'(z) = q_0' \cdot \cos\left(\frac{\pi z}{H_e} \right)$$

q_0' = peak linear heat generation rate in the fuel pin, at $z = 0$ ($W \cdot m^{-1}$)

H = total fuel zone height (m)

H_e = extrapolated height of the fuel zone (m)

$R_g = \left(R_{fo} + R_{ci} \right) / 2$ = average gas gap radius (m)

R_{fo} = fuel meat outer radius (m)

R_{ci} = cladding inner radius (m)

R_{co} = cladding outer radius (m)

h_g = gas gap conductance ($W \cdot m^{-2} \cdot K^{-1}$)

k_c = cladding thermal conductivity ($W \cdot m^{-1} \cdot K^{-1}$)
h_{Na} = sodium coolant heat transfer coefficient ($W \cdot m^{-2} \cdot K^{-1}$)
$T_m(z)$ = axial temperature profile of the mean coolant temperature at the cladding interface (K)

$$T_m(z) = T_{inlet} + a\left[\sin\left(\frac{\pi z}{H}\right) + 1\right]$$

T_{inlet} = coolant temperature at the cold inlet (K)
a = a coefficient defined by the coolant mass flow rate, coolant heat capacity, and channel height

The combination of an axial "chopped cosine" power profile in the fuel meat and a sine-shaped axial temperature profile in the flowing coolant results in an axial temperature profile at the fuel meat surface with a "lopsided cosine" shape as shown in Figure 11 (solid purple line). One may then generate an idealized hydrogen content axial profile by minimizing the hydrogen dissociation pressure (Equation 17) along the height of the fuel zone (green dotted line). Assuming that metal hydride fuel pellets are fabricated with approximately homogeneous hydrogen content, the fuel pin fresh fuel configuration will initially have discontinuous axial hydrogen concentrations from pellet to pellet as a function of fuel zone height, represented by the vertical lines in Figure 11 (where 10 vertical pellets shown represent the 10 fuel pellets in this hypothetical fuel rod). Note that Figure 11 is for illustrative purposes only and has not been optimized for any particular reactor design/conditions.

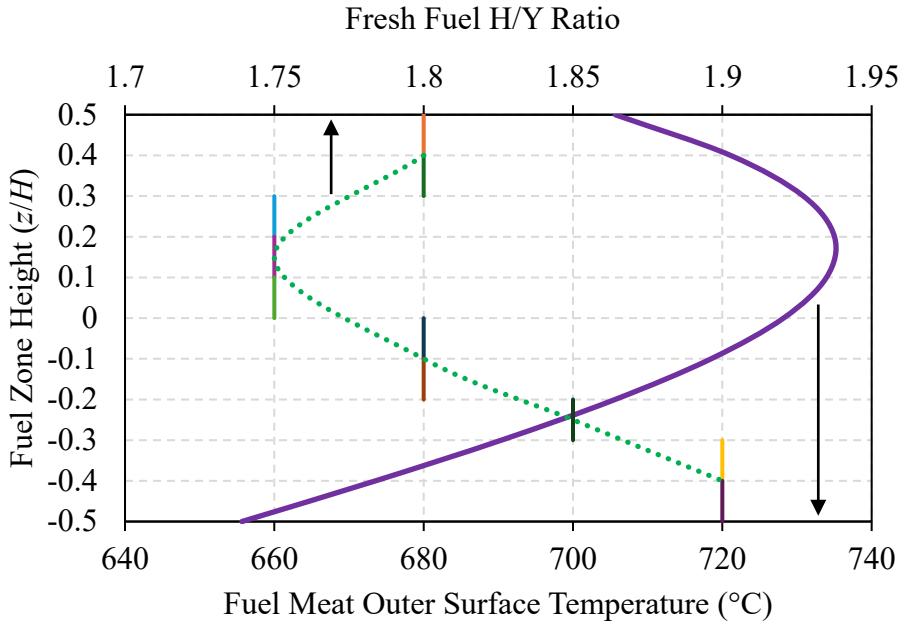

Figure 11: Example of an axial temperature profile of the fuel meat outer surface in the fuel pin (solid purple line), and an idealized hydrogen composition axial profile to enable an approximately constant axial hydrogen dissociation pressure at the fuel meat surface (green dotted line). If hydride fuel pellets are manufactured with relatively homogeneous hydrogen content, this results in a discontinuous as-fabricated hydrogen content axial profile, represented by 10 such fuel pellets illustrated here (vertical lines).

5.3 Other Considerations

Fission products are not expected to preferentially bond with hydrogen (or oxygen impurities in the fuel meat) in U-YH_x fuel because yttrium hydride and yttrium oxide bonds are remarkably thermodynamically stable [46]. This means that, unlike in U-ZrH_x fuel [3], the H/Y ratio in the U-YH_x is not expected to evolve as fission products are produced. However, the number of yttrium atoms in the fuel will change over time to some extent due to other nuclear reactions. Unlike zirconium, yttrium only has one stable isotope (^{89}Y), and ^{90}Y notably has a half-life of only 65 hours. This means that yttrium neutron absorption results in a decrease in yttrium population in the metal hydride matrix (note that this is also true for yttrium hydride solid moderator elements which don't contain uranium). Conversely, the number of ^{89}Y atoms will increase over time as a result of ^{89}Y fission product accumulation (both directly born from fission and as a result of radioactive decay from other fission product precursors). For a simple first order approximation, the rate at which the ^{89}Y inventory changes during steady state operation can be calculated analytically using Equation 25 where it has been approximated that ^{89}Y neutron absorption immediately results in a loss of yttrium due to the short ^{90}Y half-life. Equation 25 is an ordinary differential equation whose analytical solution is given by Equation 26. The integrals in Equation 26 may be replaced by appropriately averaged fission yield and neutron absorption constants as shown in Equation 27, but doing so requires knowledge of the neutron energy spectrum for the specific reactor of interest.

$$[\textit{Change Rate}] = [\textit{Gain Rate}] - [\textit{Loss Rate}]$$

$$\therefore$$

$$\frac{dN_{Y-89}}{dt} \approx \dot{F}\int \zeta_{Y-89}(E)dE - N_{Y-89}(t)\cdot\int \phi(E)\cdot\sigma_a(E)\,dE \qquad \text{Equation 25}$$

Where
$N_{Y\text{-}89}(t)$ = ^{89}Y atom density at time t (atoms·cm^{-3})
$\dot{F}$ = fission density rate in the fuel meat (fissions·cm^{-3}·s^{-1})
$\zeta_{Y-89}(E)$ = energy-dependent fission yield of ^{89}Y atoms (atoms·fission^{-1})
$\phi(E)$ = energy-dependent neutron flux (neutrons·cm^{-2}·s^{-1})
$\sigma_a(E)$ = energy-dependent neutron absorption cross section of ^{89}Y (cm^2·neutron^{-1})
t = time (s)
E = neutron energy (eV)

$$N_{Y-89}(t) \approx \frac{\dot{F}\int \zeta_{Y-89}(E)dE}{\int \phi(E)\cdot\sigma_a(E)\,dE} + e^{-t\int \phi(E)\cdot\sigma_a(E)dE}\cdot\left(N_{Y,0} - \frac{\dot{F}\int \zeta_{Y-89}(E)dE}{\int \phi(E)\cdot\sigma_a(E)\,dE}\right) \qquad \text{Equation 26}$$

Where
$N_{Y,0}$ = ^{89}Y atom density in the as-fabricated condition (atoms·cm^{-3}), see Equation 2

$$N_{Y-89}(t) \approx \frac{\dot{F}\cdot\zeta_{Y-89,avg}}{\phi_{avg}\cdot\sigma_{a,avg}} + e^{-t\cdot\phi_{avg}\cdot\sigma_{a,avg}}\cdot\left(N_{Y,0} - \frac{\dot{F}\cdot\zeta_{Y-89,avg}}{\phi_{avg}\cdot\sigma_{a,avg}}\right) \qquad \text{Equation 27}$$

Where
$N_{Y\text{-}89}(t)$ = ^{89}Y atom density in the fuel meat at time t (atoms·cm^{-3})
$\dot{F}$ = fission density rate in the fuel meat (fissions·cm^{-3}·s^{-1})
$\zeta_{Y-89,avg}$ = energy-averaged fission yield of ^{89}Y atoms (atoms·fission^{-1})
ϕ_{avg} = energy-averaged neutron flux (neutrons·cm^{-2}·s^{-1})
$\sigma_{a,avg}$ = energy-averaged neutron absorption cross section of ^{89}Y (cm^2·neutron^{-1})
$N_{Y,0}$ = ^{89}Y atom density in the as-fabricated condition (atoms·cm^{-3}), see Equation 2
t = time (s)

The average H/Y ratio in the metal hydride at time t due only to nuclear reactions (i.e., ignoring hydrogen dissociation and leakage) is given by Equation 28 [3]. For a sense of scale, consider the fuel described in Table 1 in a hypothetical system where all the neutrons are thermal (having kinetic energy equal to 0.0235 eV). The cumulative fission yield for ^{89}Y due to thermal neutrons is roughly $\zeta_{Y\text{-}89} \approx 0.048$ atoms per thermal fission of ^{235}U, while the thermal neutron absorption cross section of ^{89}Y is about $\sigma_a \approx 1.3 \cdot 10^{-24}$ cm^2 [47]. Assuming a neutron flux (all thermal) of $\phi = 10^{14}$ neutrons·cm^{-2}·s^{-1} and a fission rate density of $\dot{F} = 5.89 \cdot 10^{12}$ fis·cm^{-3}·s^{-1} (approximately representative of the power density in Table 1), Equation 27 predicts that the ^{89}Y atom density in the fuel meat will drop from $2.6361 \cdot 10^{22}$ atoms·cm^{-3} to $2.6016 \cdot 10^{22}$ atoms·cm^{-3} after the full 3.5 year fuel cycle (a decrease by about 1%). Using Equation 28, this yields an average H/Y increase from $x_{avg} = 1.800$ to 1.801 at EOL, an entirely negligible change from a hydride phase stability perspective. The H/Y ratio increased in this example, indicating that the yttrium population gain rate (due primarily to fission product precursors decaying into ^{89}Y) is less than the rate that ^{89}Y absorbs neutrons. However, real nuclear reactors do not contain monoenergetic neutron fluxes. Microreactors in particular are more compact and may have slightly epithermally-shifted neutron energy spectra, as is the case for the MARVEL reactor [1]. In real reactor systems, the true yttrium evolution due to nuclear reactions may be different. The ^{89}Y yield changes very little with energy (down to about 0.045 at 1 MeV) in comparison to the ^{89}Y neutron absorption cross section which changes by several orders of magnitude as shown in Figure 12 [47]. The absorption cross section decreases as neutron energy increases until the resonance range begins at around 2.6 keV.

$$x(t)\Big]_f = \frac{x_0}{1 + \left(\frac{N_{Y-89}(t) - N_{Y,0}}{N_A} \right)} \qquad \text{Equation 28}$$

Where
$x(t)\Big]_f$ = average H/Y ratio at time t due to fission-induced evolution effects only (atoms·cm^{-3}·s^{-1})
x_0 = initial H/Y ratio
$N_{Y\text{-}89}(t)$ = ^{89}Y atom density in the fuel meat at time t (atoms·cm^{-3}), see Equation 26
N_A = Avogadro's number = $6.022 \cdot 10^{23}$ (atoms·mol^{-1})
$N_{Y,0}$ = ^{89}Y atom density in the as-fabricated condition (atoms·cm^{-3}), see Equation 2
t = time (s)

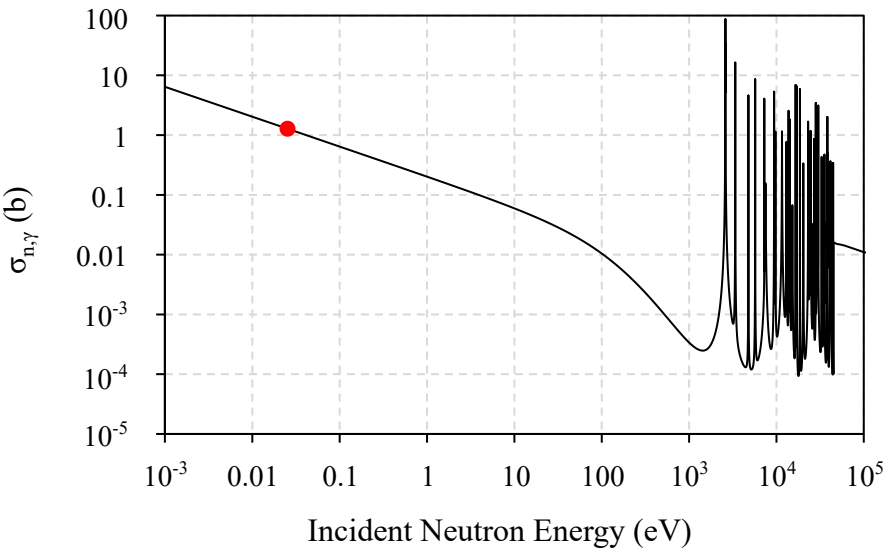

Figure 12: Radiative neutron capture cross section spectrum of ^{89}Y in units of barns (1 b = 10^{-24} cm^2). The red dot represents the cross section for thermal neutrons (0.0253 eV).

6. CONCLUSIONS

In this study, we consider the properties and relationships relevant to hydride stability associated with the hypothetical nuclear fuel system uranium-yttrium hydride that has been stabilized for use in extreme conditions using advanced manufacturing techniques [14-18] (the experimental details of which will be revealed in a forthcoming manuscript). If successfully stabilized, the U-YH_x nuclear fuel system would represent a high temperature, high burnup analogue to the well-known U-ZrH_x fuel system due to yttrium hydride's superior thermodynamic stability and ability to retain hydrogen at high temperatures. Even at H/Y = 1.80, the hydrogen dissociation pressure in the fuel pin is nearly three orders of magnitude less than that of U-$ZrH_{1.60}$ under equivalent thermal conditions (see Figure 4). However, the Soret heat of transport, which is the key parameter describing the sensitivity to thermophoretic transport of hydrogen, has never been measured for δ-YH_x. One of the primary objectives of this study is to determine the sensitivity of key hydrogen-related properties in this material to the Soret heat of transport. Since the Soret effect is driven by temperature gradients, a case with a large temperature gradient was considered there: the temperature profile of a yttrium hydride-based nuclear fuel candidate operating at commercially relevant high power density (see Table 1) in a prototypic high temperature sodium-cooled microreactor.

This sensitivity study involved varying the δ-YH_x Soret heat of transport temperature, T_Q (normally assumed to be equal to that of δ-ZrH_x, which is 640 K), from 300 K to 1000 K. Even though the total magnitude of hydrogen redistribution variation is small over this T_Q range (up to 2%), the hydrogen dissociation pressure dependence upon hydrogen concentration is non-linear, resulting in pressure variations up to 16% over the considered T_Q range. This resulted in a hydrogen leakage rate (through the cladding, into the primary coolant) which varies by up to about 8% depending on the value of T_Q. While these uncertainties are large, this results in an EOL x_{avg} variation of up to only 0.05% due to yttrium hydride's exceptional ability to retain hydrogen at high temperatures. In conclusion, we find that hydride stability analyses under prototypic full power operating conditions in a commercial-scale sodium-cooled microreactor are insensitive to

the assumed value of T_Q. However, the hydrogen dissociation pressure (Equation 17) is also a non-linear function of temperature, meaning that the assumed value of T_Q will be more sensitive to the determined operational limits of a yttrium hydride-based nuclear fuel pin. In quantifying the sensitivity of hydrogen behavior to the selection of the assumed value of T_Q for this novel fuel system, this work enables forthcoming studies that are more encompassing to the broader scope of fuel performance behavior.

Other properties and parameters related to the performance of yttrium hydride-based fuel are also discussed. Similar to other metal hydride-based fuel element analogues (ex. TRIGA and MARVEL), the axial redistribution of hydrogen within the metal hydride pin will be significantly reduced by loading the fuel pin with an axial composition gradient to counteract the anticipated temperature gradient from the start. First order analytical calculations were also performed which suggest that the H/Y ratio is insensitive to fission product and nuclear transmutation reactions.

DECLARATION OF COMPETING INTERESTS

The authors declare that they have no known competing financial interests or personal relationships that could have appeared to influence the work reported in this paper.

ACKNOWLEDGEMENTS

This work was supported through the INL Laboratory Directed Research & Development (LDRD) Program under Department of Energy (DOE) Idaho Operations Office Contract DE-AC07-05ID14517. The United States Government retains and the publisher, by accepting the article for publication, acknowledges that the United States Government retains a nonexclusive, royalty-free, paid-up, irrevocable, world-wide license to publish or reproduce the published form of this manuscript, or allow others to do so, for United States Government purposes. The authors wish to thank Dr. John Jackson, National Technical Director of the Department of Energy Office of Nuclear Energy (DOE-NE) Microreactor Program, for his time and engaging discussions related to applying this emergent technology to nuclear powered microreactors.

REFERENCES

[1] T. Lange, A. Wagner, C. Parisi, Y. Arafat, MARVEL Core Design and Neutronic Characteristics, Transactions of the American Nuclear Society 127 (2022) 1078-1081.
[2] J.A. Evans, C. Parisi, Optimizing Hydride Stability in U-ZrH Nuclear Fuel: The "Goldilocks Radius", Nucl Sci Eng (2024).
[3] J.A. Evans, R.T. Sweet, P.G. Medvedev, A.R. Wagner, C. Parisi, T.L. Lange, E. Perez, F. Rice, J.F. Jue, E. Woolstenhulme, D.J.r. Keiser, Y. Arafat, Uranium-zirconium hydride nuclear fuel performance in the NaK-cooled MARVEL microreactor, J Nucl Mater 598 (2024).
[4] W.E. Wang, D.R. Olander, Thermodynamics of the Zr-H system, J Am Ceram Soc 78(12) (1995) 3323-3328.
[5] A.P. Shivprasad, D.M. Frazer, V.K. Mehta, M.W.D. Cooper, T.A. Saleh, J.T. White, J.R. Wermer, E.P. Luther, D.V. Rao, Elastic moduli of high-density, sintered monoliths of yttrium dihydride, J Alloy Compd 826 (2020).
[6] A.P. Shivprasad, S.C. Vogel, V.K. Mehta, M.W.D. Cooper, T.A. Saleh, J.T. White, J.R. Wermer, E.P. Luther, H.R. Trellue, Thermophysical properties of high-density, sintered monoliths of yttrium dihydride in the range 373-773 K, J Alloy Compd 850 (2021).

[7] H. Trellue, C. Taylor, E. Luther, T. Cutler, A. Shivprasad, J.K. Jewell, D.V. Rao, M. Davenport, Advancements in Yttrium Hydride Moderator Development, Nucl Technol 209 (2023) S123-S135.
[8] A.P. Shivprasad, E.P. Luther, V.R. Dasari, Hydrogen loss from clad metal hydride moderators, LA-UR-22-21195, Los Alamos National Laboratory, USDOE Office of Nuclear Energy. https://www.osti.gov/biblio/1874905, (2022).
[9] B.J. Ade, B.R. Betzler, J.R. Burns, C.W. Chapman, J.W. Hu, Reactor Physics Considerations for Use of Yttrium Hydride Moderator, Nucl Sci Eng 196(12) (2022) 1539-1558.
[10] N. Woolstenhulme, J. Evans, A. Chipman, R. Armstrong, Nuclear fuels for transient test reactors, Ann Nucl Energy 204 (2024).
[11] R.I. Sheldon, D.E. Peterson, The U-Zr (Uranium-Zirconium) System, Bulletin of Alloy Phase Diagrams 10(2) (1989) 165-171.
[12] T.B. Massalski, Binary Alloy Phase Diagrams, Second Edition, Materials Information Soc., Materials Park, Ohio, 1990.
[13] P. Duenner, D. Becker, Development work for the moderator of the ITR-fuel, IA-ITB--73.42, International Atomic Energy Agency, Bergisch Gladbach, Germany, 1973.
[14] V.H. Hammond, B.C. Hornbuckle, A.K. Giri, A.J. Roberts, T.L. Luckenbaugh, J.M. Marsico, S.M. Grendahl, K.A. Darling, Processing of Bulk Nanocrystalline Metals at the US Army Research Laboratory, Jove-J Vis Exp (133) (2018).
[15] K.A. Darling, M.A. Tschopp, R.K. Guduru, W.H. Yin, Q. Wei, L.J. Kecskes, Microstructure and mechanical properties of bulk nanostructured Cu-Ta alloys consolidated by equal channel angular extrusion, Acta Mater 76 (2014) 168-185.
[16] M.A. Tschopp, H.A. Murdoch, L.J. Kecskes, K.A. Darling, "Bulk" Nanocrystalline Metals: Review of the Current State of the Art and Future Opportunities for Copper and Copper Alloys, Jom-Us 66(6) (2014) 1000-1019.
[17] P.V. Patki, Y.Q. Wu, J. Wharry, Effects of proton irradiation on microstructure and mechanical properties of nanocrystalline Cu-10at%Ta alloy, Materialia 9 (2020).
[18] N.Q. Vo, S.W. Chee, D. Schwen, X.A. Zhang, P. Bellon, R.S. Averback, Microstructural stability of nanostructured Cu alloys during high-temperature irradiation, Scripta Mater 63(9) (2010) 929-932.
[19] S. Terlizzi, V. Labouré, Asymptotic hydrogen redistribution analysis in yttrium-hydride-moderated heat-pipe-cooled microreactors using DireWolf, Ann Nucl Energy 186 (2023).
[20] X.X. Hu, K.A. Terrani, Thermomechanical properties and microstructures of yttrium hydride, J Alloy Compd 867 (2021).
[21] D.L. Lindner, Isothermal Decomposition of Uranium Hydride, J Less-Common Met 157(1) (1990) 139-146.
[22] D. Olander, E. Greenspan, H.D. Garkisch, B. Petrovic, Uranium-zirconium hydride fuel properties, Nucl Eng Des 239(8) (2009) 1406-1424.
[23] D.R. Olander, M. Ng, Hydride fuel behavior in LWRs, J Nucl Mater 346(2-3) (2005) 98-108.
[24] M.S. El-Genk, Deployment history and design considerations for space reactor power systems, Acta Astronaut 64(9-10) (2009) 833-849.
[25] J. Katz, E. Rabinowitch, The Chemistry of Uranium, p. 177, Division VIII, Vol. 5, National Nuclear Energy Series, McGraw-Hill Book Company, Inc., New York, 1951.
[26] T.B. Douglas, A Cryoscopic Study of the Solubility of Uranium in Liquid Sodium at 97.8-Degrees-C, J Res Nat Bur Stand 52(5) (1954) 223-226.
[27] J. Vetrano, Delta-Phase Zirconium Hydride as a Solid Moderator, BMI-1243, Battelle Memorial Institute, Columbus, Ohio, 1957.

[28] N.E. Todreas, M.S. Kazimi, Nuclear Systems I: Thermal Hydraulic Fundamentals, Taylor & Francis1990.
[29] D.J.r. Keiser, J.F. Jue, F. Rice, E. Woolstenhulme, Post irradiation examination of a uranium-zirconium hydride TRIGA fuel element, Front Energy Res 11 (2023).
[30] NUREG-1282, Safety Evaluation Report on High-Uranium Content, Low-Enriched Uranium-Zirconium Hydride Fuels for TRIGA Reactors, U.S. Nuclear Regulatory Commission, Office of Nuclear Reactor Regulation, 1987.
[31] M.T. Mustafa, A.F.M. Arif, K. Masood, Approximate Analytic Solutions of Transient Nonlinear Heat Conduction with Temperature-Dependent Thermal Diffusivity, Abstr Appl Anal (2014).
[32] A. Khanolkar, M.N. Cinbiz, J.G. Yu, X.X. Hu, High temperature elastic properties of sub-stoichiometric yttrium dihydrides*, Mater Today Commun 35 (2023).
[33] Thermophysical Properties of Materials For Nuclear Engineering: A Tutorial and Collection of Data, Nuclear Power Technology Development Section International Atomic Energy Agency. Vienna, Austria, 2008.
[34] K.Y. Spencer, L. Sudderth, R.A. Brito, J.A. Evans, C.S. Hart, A.B. Hu, A. Jati, K. Stern, S.M. McDeavitt, Sensitivity study for accident tolerant fuels: Property comparisons and behavior simulations in a simplified PWR to enable ATF development and design, Nucl Eng Des 309 (2016) 197-212.
[35] A.A. Trofimov, X.X. Hu, H. Wang, Y. Yang, K.A. Terrani, Thermophysical properties and reversible phase transitions in yttrium hydride, J Nucl Mater 542 (2020).
[36] S. Yamanaka, K. Yamada, K. Kurosaki, M. Uno, K. Takeda, H. Anada, T. Matsuda, S. Kobayashi, Thermal properties of zirconium hydride, J Nucl Mater 294(1-2) (2001) 94-98.
[37] S. Yamanaka, K. Yoshioka, M. Uno, M. Katsura, H. Anada, T. Matsuda, S. Kobayashi, Thermal and mechanical properties of zirconium hydride, J Alloy Compd 293 (1999) 23-29.
[38] J.Q. Peng, M. Wu, F. Du, F.L. Yang, J.Y. Shen, L.J. Wang, X.Y. Ye, G.Q. Yan, Thermodynamic modelling of Y-H and Y-Zr-H system aided by first-principles and its application in bulk hydride moderator fabrication, J Nucl Mater 531 (2020).
[39] A.T. Motta, L. Capolungo, L.Q. Chen, M.N. Cinbiz, M.R. Daymond, D.A. Koss, E. Lacroix, G. Pastore, P.C.A. Simon, M.R. Tonks, B.D. Wirth, M.A. Zikry, Hydrogen in zirconium alloys: A review, J Nucl Mater 518 (2019) 440-460.
[40] D. Khatamian, F.D. Manchester, The H-Y (Hydrogen-Yttrium) System, Bulletin of Alloy Phase Diagrams 9(3) (1988) 252-260.
[41] C.E. Lundin, J.P. Blackledge, Pressure-Temperature-Composition Relationships of the Yttrium-Hydrogen System, J Electrochem Soc 109(9) (1962) 838-842.
[42] S. Masashi, Tritium Transport in Fusion Reactor Materials. In: Konings, Rudy JM and Stoller Roger E (eds.), Comprehensive Nuclear Materials, 2nd Edition, Elsevier, Oxford, 2020.
[43] R.L. Williamson, J.D. Hales, S.R. Novascone, G. Pastore, K.A. Gamble, B.W. Spencer, W. Jiang, S.A. Pitts, A. Casagranda, D. Schwen, A.X. Zabriskie, A. Toptan, R. Gardner, C. Matthews, W.F. Liu, H.L. Chen, BISON: A Flexible Code for Advanced Simulation of the Performance of Multiple Nuclear Fuel Forms, Nucl Technol 207(7) (2021) 954-980.
[44] M.A. Tunes, D. Parkison, Y. Huang, M.R. Chancey, S.C. Vogel, V.K. Mehta, M.A. Torrez, E.P. Luther, J.A. Valdez, Y. Wang, J. Yu, M.N. Cinbiz, A.P. Shivprasad, C.A. Kohnert, Challenges in developing materials for microreactors: A case-study of yttrium dihydride in extreme conditions, Acta Mater 280 (2024).

[45] M.T. Simnad, G.B. West, J.D. Randall, W.J. Richards, D. Stahl, Interpretation of Damage to the FLIP Fuel During Operation of the Nuclear Science Center Reactor at Texas A&M University, GA-A16613, GA Technologies, 1981.
[46] J.T. Huang, B. Tsuchiya, K. Konashi, M. Yamawaki, Thermodynamic analysis of chemical states of fission products in uranium-zirconium hydride fuel, J Nucl Mater 294(1-2) (2001) 154-159.
[47] M.B. Chadwick, M. Herman, e.a. P. Oblozinsky, ENDF/B-VII.1 Nuclear Data for Science and Technology: Cross Sections, Covariances, Fission Product Yields, and Decay Data, Nuclear Data Sheets, 112(12):2887-2996, 2011.